

We are IntechOpen, the world's leading publisher of Open Access books Built by scientists, for scientists

6,900

Open access books available

185,000

International authors and editors

200M

Downloads

Our authors are among the

154

Countries delivered to

TOP 1%

most cited scientists

12.2%

Contributors from top 500 universities



WEB OF SCIENCE™

Selection of our books indexed in the Book Citation Index
in Web of Science™ Core Collection (BKCI)

Interested in publishing with us?
Contact book.department@intechopen.com

Numbers displayed above are based on latest data collected.
For more information visit www.intechopen.com



The Influence of the Dielectric Materials on the Fields in the Millimeter and Infrared Wave Regimes

Zion Menachem

Abstract

This chapter presents the influence of the dielectric materials on the output field for the millimeter and infrared regimes. This chapter presents seven examples of the discontinuous problems in the cross section of the straight waveguide. Two different geometrical of the dielectric profiles in the cross section of the straight rectangular and circular waveguides will be proposed to understand the behavior of the output fields. The two different methods for rectangular and circular waveguides and the techniques to calculate any geometry in the cross section are very important to understand the influence of the dielectric materials on the output fields. The two different methods are based on Laplace and Fourier transforms and the inverse Laplace and Fourier transforms. Laplace transform on the differential wave equations is needed to obtain the wave equations and the output fields that are expressed directly as functions of the transmitted fields at the entrance of the waveguide. Thus, the Laplace transform is necessary to obtain the comfortable and simple *input-output* connections of the fields. The applications are useful for straight waveguides in the millimeter and infrared wave regimes.

Keywords: wave propagation, dielectric profiles, rectangular and circular waveguides, dielectric materials

1. Introduction

Various methods for analysis of waveguides have been studied in the literature. The review for the modal analysis of general methods has been published [1]. The important methods, such as the finite difference method and integral equation method, and methods based on series expansion have been described. An analytical model for the corrugated rectangular waveguide has been extended to compute the dispersion and interaction impedance [2]. The application of analytical method based on the field equations has been presented to design corrugated rectangular waveguide slow-wave structure TH_z amplifiers.

A fundamental technique has been proposed to compute the propagation constant of waves in a lossy rectangular waveguide [3]. An important consequence of this work is the demonstration that the loss computed for degenerate modes propagating simultaneously is not simply additive. The electromagnetic fields in

rectangular conducting waveguides filled with uniaxial anisotropic media have been characterized [4].

A full-vectorial boundary integral equation method for computing guided modes of optical waveguides has been proposed [5]. The integral equations are used to compute the Neumann-to-Dirichlet operators for sub-domains of constant refractive index on the transverse plane of the waveguide. Wave propagation in an inhomogeneous transversely magnetized rectangular waveguide has been studied with the aid of a modified Sturm-Liouville differential equation [6].

An advantageous finite element method for the rectangular waveguide problem has been developed [7] by which complex propagation characteristics may be obtained for arbitrarily shaped waveguide. The characteristic impedance of the fundamental mode in a rectangular waveguide was computed using finite element method. The finite element method has been used to derive approximate values of the possible propagation constant for each frequency. A new structure has been proposed for microwave filters [8]. This structure utilizes a waveguide filled by several dielectric layers. The relative electric permittivity and the length of the layers were optimally obtained using least mean square method.

An interesting method has been introduced for frequency domain analysis of arbitrary longitudinally inhomogeneous waveguides [9]. In this method, the integral equations of the longitudinally inhomogeneous waveguides are converted from their differential equations and solved using the method of moments. A general method has been introduced to frequency domain analysis of longitudinally inhomogeneous waveguides [10]. In this method, the electric permittivity and also the transverse electric and magnetic fields were expanded in Taylor's series. The field solutions were obtained after finding unknown coefficients of the series. A general method has been introduced to analyze aperiodic or periodic longitudinally inhomogeneous waveguides [11]. The periodic longitudinally inhomogeneous waveguides were analyzed using the Fourier series expansion of the electric permittivity function to find their propagation constant and characteristic impedances.

Various methods for the analysis of cylindrical hollow metallic or metallic with inner dielectric coating waveguide have been studied in the literature. A review of the hollow waveguide technology [12, 13] and a review of IR transmitting, hollow waveguides, fibers, and integrated optics [14] were published. Hollow waveguides with both metallic and dielectric internal layers have been proposed to reduce the transmission losses. A hollow waveguide can be made, in principle, from any flexible or rigid tube (plastic, glass, metal, etc.) if its inner hollow surface (the core) is covered by a metallic layer and a dielectric overlayer. This layer structure enables us to transmit both the TE and TM polarizations with low attenuation [15].

A transfer matrix function for the analysis of electromagnetic wave propagation along the straight dielectric waveguide with arbitrary profiles has been proposed [16]. This method is based on the Laplace and Fourier transforms. This method is based on Fourier coefficients of the transverse dielectric profile and those of the input-wave profile. Laplace transform is necessary to obtain the comfortable and simple input-output connections of the fields. The transverse field profiles are computed by the inverse Laplace and Fourier transforms.

The influence of the spot size and cross section on the output fields and power density along the straight hollow waveguide has been proposed [17]. The derivation is based on Maxwell's equations. The longitudinal components of the fields are developed into the Fourier-Bessel series. The transverse components of the fields are expressed as functions of the longitudinal components in the Laplace plane and are obtained by using the inverse Laplace transform by the residue method.

These are two kinds of different methods that enable us to solve practical problems with different boundary conditions. The calculations in all methods are based on using Laplace and Fourier transforms, and the output fields are computed by the inverse Laplace and Fourier transforms. Laplace transform on the differential wave equations is needed to obtain the wave equations (and thus also the output fields) that are expressed directly as functions of the transmitted fields at the entrance of the waveguide at $z = 0^+$. Thus, the Laplace transform is necessary to obtain the comfortable and simple *input-output* connections of the fields.

All models that are mentioned refer to solve interesting wave propagation problems with a particular geometry. If we want to solve more complex discontinuous problems of coatings in the cross section of the dielectric waveguides, then it is important to develop for each problem an improved technique for calculating the profiles with the dielectric material in the cross section of the straight waveguide.

This chapter presents two techniques for two different geometries of the straight waveguide. The two proposed techniques are very important to solve discontinuous problems with dielectric material in the cross section of the straight rectangular and circular waveguides. The proposed technique relates to the method for the propagation along the straight rectangular metallic waveguide [16]. The examples will be demonstrated for the rectangular and circular dielectric profiles in the straight rectangular waveguide.

In this chapter, we present seven dielectric structures as shown in **Figure 1(a)–(g)**. **Figure 1(a)–(e)** shows five examples of the discontinuous dielectric materials in the cross section of the rectangular straight waveguide. **Figure 1(f)–(g)** shows two examples of the discontinuous dielectric materials in the cross section of the circular straight waveguide.

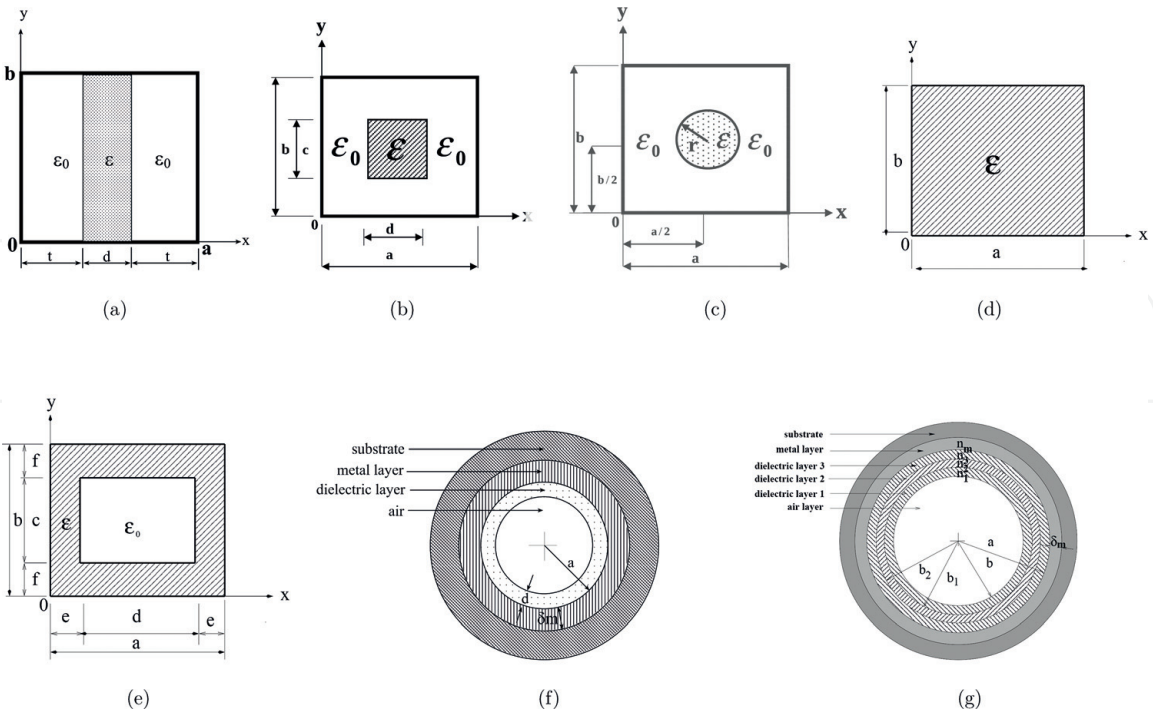


Figure 1. Seven examples of dielectric materials in the cross section of the straight waveguides. (a) Slab profile in the cross section of the straight waveguides. (b) Rectangular profile in the rectangular waveguide. (c) Circular profile in the rectangular waveguide. (d) Full dielectric material in the rectangular waveguide. (e) Hollow rectangular waveguide with one dielectric material between the hollow rectangle and the metal. (f) Hollow waveguide with one dielectric coating. (g) Hollow waveguide with three dielectric coatings.

2. Two proposed techniques for discontinuous problems in the cross section of the rectangular and circular waveguides

The wave equations for the components of the electric and magnetic field are given by

$$\nabla^2 E + \omega^2 \mu \epsilon E + \nabla \left(E \cdot \frac{\nabla \epsilon}{\epsilon} \right) = 0 \quad (1)$$

and

$$\nabla^2 H + \omega^2 \mu \epsilon H + \frac{\nabla \epsilon}{\epsilon} \times (\nabla \times H) = 0 \quad (2)$$

where ϵ_0 represents the vacuum dielectric constant, χ_0 is the susceptibility, and g is its dielectric profile function in the waveguide.

Let us introduce the dielectric profile function for the examples as shown in **Figure 1(a)–(g)** for the inhomogeneous dielectric materials.

3. The derivation for rectangular straight waveguide

The wave Eqs. (1) and (2) are given in the case of the rectangular straight waveguide, where

$$\epsilon(x, y) = \epsilon_0(1 + \chi_0 g(x, y)), \quad g_x = [1/\epsilon(x, y)][\partial \epsilon(x, y)/\partial x], \text{ and} \\ g_y = [1/\epsilon(x, y)][\partial \epsilon(x, y)/\partial y].$$

3.1 The first technique to calculate the discontinuous structure of the cross section

Figure 2(a) shows an example of the cross section of the straight waveguide (**Figure 1(a)**) for $g(x)$ function. In order to solve inhomogeneous dielectric profiles, we use the ω_ϵ function, with the parameters ϵ_1 and ϵ_2 (**Figures 1(a)** and **(b)**).

The ω_ϵ function [18] is used in order to solve discontinuous problems in the cross section of the straight waveguide. The ω_ϵ function is defined according to **Figure 2(b)** as

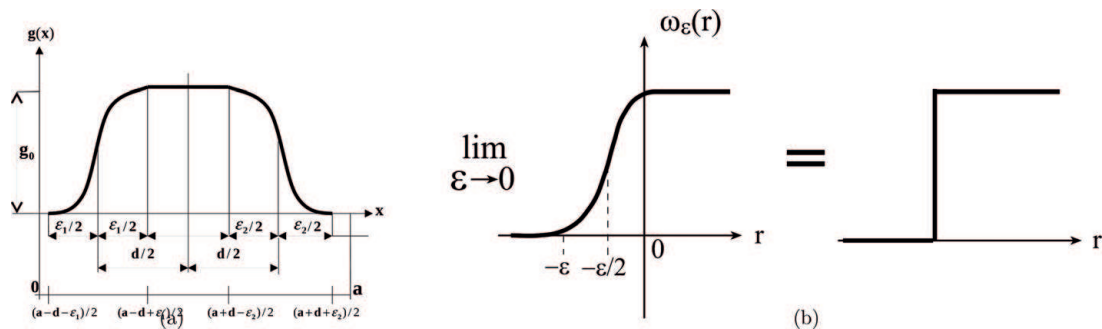


Figure 2.

(a) An example of the discontinuous problem of the slab dielectric profile in the straight rectangular waveguide.
(b) The ω_ϵ function in the limit $\epsilon \rightarrow 0$.

$$\omega_\varepsilon(r) = \begin{cases} C_\varepsilon e^{-\frac{\varepsilon^2}{\varepsilon^2 - |r|^2}} & |r| \leq \varepsilon, \\ 0 & |r| > \varepsilon \end{cases}, \quad (3)$$

where C_ε is a constant and $\int \omega_\varepsilon(r) dr = 1$.

In order to solve inhomogeneous dielectric profiles (e.g., in **Figure 1(a)–(b)**) in the cross section of the straight waveguide, the parameter ε is used according to the ω_ε function (**Figure 2(b)**), where $\varepsilon \rightarrow 0$. The dielectric profile in this case of a rectangular dielectric material in the rectangular cross section (**Figure 1(b)**) is given by

$$g(x) = \begin{cases} 0 & 0 \leq x < (a - d - \varepsilon)/2 \\ g_0 \exp \left[1 - \frac{\varepsilon^2}{\varepsilon^2 - [x - (a - d + \varepsilon)/2]^2} \right] & (a - d - \varepsilon)/2 \leq x < (a - d + \varepsilon)/2 \\ g_0 & (a - d + \varepsilon)/2 < x < (a + d - \varepsilon)/2, \\ g_0 \exp \left[1 - \frac{\varepsilon^2}{\varepsilon^2 - [x - (a + d - \varepsilon)/2]^2} \right] & (a + d - \varepsilon)/2 \leq x < (a + d + \varepsilon)/2 \\ 0 & (a + d + \varepsilon)/2 < x \leq a \end{cases} \quad (4)$$

and

$$g(y) = \begin{cases} 0 & 0 \leq y < (b - c - \varepsilon)/2 \\ g_0 \exp \left[1 - \frac{\varepsilon^2}{\varepsilon^2 - [y - (b - c + \varepsilon)/2]^2} \right] & (b - c - \varepsilon)/2 \leq y < (b - c + \varepsilon)/2 \\ g_0 & (b - c + \varepsilon)/2 < y < (b + c - \varepsilon)/2. \\ g_0 \exp \left[1 - \frac{\varepsilon^2}{\varepsilon^2 - [y - (b + c - \varepsilon)/2]^2} \right] & (b + c - \varepsilon)/2 \leq y < (b + c + \varepsilon)/2 \\ 0 & (b + c + \varepsilon)/2 < y \leq b \end{cases} \quad (5)$$

The elements of the matrices are given according to **Figure 1(b)**, in the case of $b \neq c$ by

$$\begin{aligned} g(n, m) = & \frac{g_0}{ab} \left\{ \int_{(a-d-\varepsilon)/2}^{(a-d+\varepsilon)/2} \exp \left[1 - \frac{\varepsilon^2}{\varepsilon^2 - [x - (a - d + \varepsilon)/2]^2} \right] \cos \left(\frac{n\pi x}{a} \right) dx \right. \\ & + \int_{(a-d+\varepsilon)/2}^{(a+d-\varepsilon)/2} \cos \left(\frac{n\pi x}{a} \right) dx + \int_{(a+d-\varepsilon)/2}^{(a+d+\varepsilon)/2} \exp \left[1 - \frac{\varepsilon^2}{\varepsilon^2 - [x - (a + d - \varepsilon)/2]^2} \right] \cos \left(\frac{n\pi x}{a} \right) dx \Big\} \\ & \left\{ \int_{(b-c-\varepsilon)/2}^{(b-c+\varepsilon)/2} \exp \left[1 - \frac{\varepsilon^2}{\varepsilon^2 - [y - (b - c + \varepsilon)/2]^2} \right] \cos \left(\frac{m\pi y}{b} \right) dy \right. \\ & + \int_{(b-c+\varepsilon)/2}^{(b+c-\varepsilon)/2} \cos \left(\frac{m\pi y}{b} \right) dy + \int_{(b+c-\varepsilon)/2}^{(b+c+\varepsilon)/2} \exp \left[1 - \frac{\varepsilon^2}{\varepsilon^2 - [y - (b + c - \varepsilon)/2]^2} \right] \cos \left(\frac{m\pi y}{b} \right) dy \Big\}, \end{aligned} \quad (6)$$

where

$$\int_{(a-d+\varepsilon)/2}^{(a+d-\varepsilon)/2} \cos\left(\frac{n\pi x}{a}\right) dx = \begin{cases} (2a/n\pi) \sin((n\pi/2a)(d-\varepsilon)) \cos((n\pi)/2) & n \neq 0 \\ d-\varepsilon & n = 0 \end{cases}$$

and

$$\int_{(b-c+\varepsilon)/2}^{(b+c-\varepsilon)/2} \cos\left(\frac{m\pi y}{b}\right) dy = \begin{cases} (2b/m\pi) \sin((m\pi/2b)(c-\varepsilon)) \cos((m\pi)/2) & m \neq 0 \\ c-\varepsilon & m = 0 \end{cases}.$$

The elements of the matrices are given according to **Figure 1(a)**, in the case of $b = c$ by

$$g(n, m) = \frac{g_0}{ab} \left\{ \int_{(a-d-\varepsilon)/2}^{(a-d+\varepsilon)/2} \exp \left[1 - \frac{\varepsilon^2}{\varepsilon^2 - [x - (a-d+\varepsilon)/2]^2} \right] \cos\left(\frac{n\pi x}{a}\right) dx \right. \\ \left. + \int_{(a-d+\varepsilon)/2}^{(a+d-\varepsilon)/2} \cos\left(\frac{n\pi x}{a}\right) dx + \int_{(a+d-\varepsilon)/2}^{(a+d+\varepsilon)/2} \exp \left[1 - \frac{\varepsilon^2}{\varepsilon^2 - [x - (a+d-\varepsilon)/2]^2} \right] \cos\left(\frac{n\pi x}{a}\right) dx \right\} \\ \left\{ \int_0^b \cos\left(\frac{m\pi y}{b}\right) dy \right\},$$

where

$$\int_0^b \cos\left(\frac{m\pi y}{b}\right) dy = (b/m\pi) \sin(m\pi) = \begin{cases} b & m = 0 \\ 0 & m \neq 0 \end{cases}.$$

3.2 The second technique to calculate the discontinuous structure of the cross section

The second technique to calculate the discontinuous structure of the cross section as shown in **Figure 1(a)** and **(b)**.

The dielectric profile $g(x, y)$ is given according to $\varepsilon(x, y) = \varepsilon_0(1 + g(x, y))$. According to **Figure 3** and for $g(x, y) = g_0$, we obtain

$$g(n, m) = \frac{g_0}{4ab} \int_{-a}^a dx \int_{-b}^b \exp[-j(k_x x + k_y y)] dy \\ = \frac{g_0}{4ab} \left\{ \int_{x_{11}}^{x_{12}} dx \int_{y_{11}}^{y_{12}} \exp[-j(k_x x + k_y y)] dy + \int_{-x_{12}}^{-x_{11}} dx \int_{y_{11}}^{y_{12}} \exp[-j(k_x x + k_y y)] dy \right. \\ \left. + \int_{-x_{12}}^{-x_{11}} dx \int_{-y_{12}}^{-y_{11}} \exp[-j(k_x x + k_y y)] dy + \int_{x_{11}}^{x_{12}} dx \int_{-y_{12}}^{-y_{11}} \exp[-j(k_x x + k_y y)] dy \right\}. \quad (7)$$

If y_{11} and y_{12} are functions of x , then we obtain

$$g(n, m) = \frac{g_0}{abk_y} \int_{x_{11}}^{x_{12}} [\sin(k_y y_{12}) - \sin(k_y y_{11})] \cos(k_x x) dx \\ = \frac{2g_0}{am\pi} \int_{x_{11}}^{x_{12}} \sin\left[\frac{k_y}{2}(y_{12} - y_{11})\right] \cos\left[\frac{k_y}{2}(y_{12} + y_{11})\right] \cos(k_x x) dx. \quad (8)$$

The dielectric profile for **Figure 1(b)** is given by

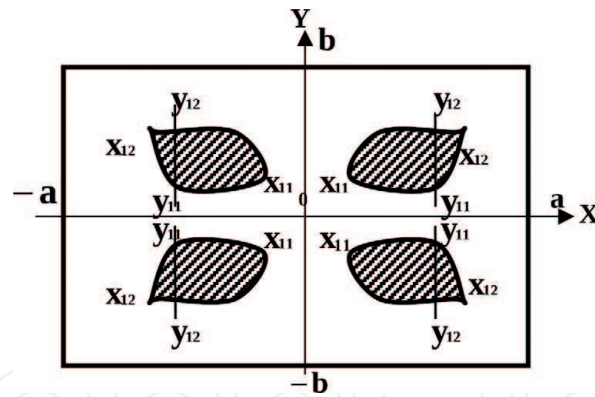


Figure 3.
The arbitrary profile in the cross section.

$$g(n, m) = \begin{cases} \frac{g_0}{4ab} (4cd) & n = 0, m = 0 \\ \frac{g_0}{4ab} \left(\frac{8d}{k_{0y}m} \sin\left(\frac{k_{0y}mc}{2}\right) \cos\left(\frac{k_{0y}mb}{2}\right) \right) & n = 0, m \neq 0 \\ \frac{g_0}{4ab} \left(\frac{8c}{k_{0x}n} \sin\left(\frac{k_{0x}nd}{2}\right) \cos\left(\frac{k_{0x}na}{2}\right) \right) & n \neq 0, m = 0 \\ \frac{g_0}{4ab} \left(\frac{16}{k_{0x}k_{0y}nm} \sin\left(\frac{k_{0x}nd}{2}\right) \cos\left(\frac{k_{0x}na}{2}\right) \sin\left(\frac{k_{0y}mc}{2}\right) \cos\left(\frac{k_{0y}mb}{2}\right) \right) & n \neq 0, m \neq 0 \end{cases} \quad (9)$$

3.3 The dielectric profile for the circular profile in the cross section

The dielectric profile for the circular profile in the cross section of the straight rectangular waveguide is given by (Figure 1(c))

$$g(x, y) = \begin{cases} g_0 & 0 \leq r < r_1 - \varepsilon/2 \\ g_0 \exp[1 - q_\varepsilon(r)] & r_1 - \varepsilon/2 \leq r < r_1 + \varepsilon/2 \end{cases} \quad (10)$$

where

$$q_\varepsilon(r) = \frac{\varepsilon^2}{\varepsilon^2 - [r - (r_1 - \varepsilon/2)]^2},$$

else $g(x, y) = 0$. The radius of the circle is given by $r = \sqrt{(x - a/2)^2 + (y - b/2)^2}$.

3.4 The dielectric profile for the waveguide filled with dielectric material in the entire cross section

The dielectric profile (Figure 1(d)) is given by

$$g(n, m) = \begin{cases} g_0 & n = 0, m = 0 \\ \frac{g_0}{4ab} \left(\frac{8a}{k_{0y}m} \sin\left(\frac{k_{0y}mb}{2}\right) \cos\left(\frac{k_{0y}mb}{2}\right) \right) & n = 0, m \neq 0 \\ \frac{g_0}{4ab} \left(\frac{8b}{k_{0x}n} \sin\left(\frac{k_{0x}na}{2}\right) \cos\left(\frac{k_{0x}na}{2}\right) \right) & n \neq 0, m = 0 \\ \frac{g_0}{4ab} \left(\frac{16}{k_{0x}k_{0y}nm} \sin\left(\frac{k_{0x}na}{2}\right) \cos\left(\frac{k_{0x}na}{2}\right) \sin\left(\frac{k_{0y}mb}{2}\right) \cos\left(\frac{k_{0y}mb}{2}\right) \right) & n \neq 0, m \neq 0 \end{cases} \quad (11)$$

3.5 The hollow rectangular waveguide with the dielectric material between the hollow rectangle and the metallic

The dielectric profile of the hollow rectangular waveguide with the dielectric material between the hollow rectangle and the metal (**Figure 1(e)**) is calculated by subtracting the dielectric profile of **Figure 1(b)** from the dielectric profile of **Figure 1(d)**.

The matrix G is given by the form

$$G = \begin{bmatrix} g_{00} & g_{-10} & g_{-20} & \cdots & g_{-nm} & \cdots & g_{-NM} \\ g_{10} & g_{00} & g_{-10} & \cdots & g_{-(n-1)m} & \cdots & g_{-(N-1)M} \\ g_{20} & g_{10} & \ddots & \ddots & \ddots & & \\ \vdots & g_{20} & \ddots & \ddots & \ddots & & \\ g_{nm} & \ddots & \ddots & \ddots & g_{00} & \vdots & \\ \vdots & & & & & & \\ g_{NM} & \cdots & \cdots & \cdots & \cdots & \cdots & g_{00} \end{bmatrix}. \quad (12)$$

Similarly, the G_x and G_y matrices are obtained by the derivatives of the dielectric profile. These matrices relate to the method that is based on the Laplace and Fourier transforms and the inverse Laplace and Fourier transforms [16]. Laplace transform is necessary to obtain the comfortable and simple input-output connections of the fields. The output transverse fields are computed by the inverse Laplace and Fourier transforms.

This method becomes an improved method by using the proposed technique and the particular application also in the cases of discontinuous problems of the hollow rectangular waveguide with dielectric material between the hollow rectangle and the metal (**Figure 1(e)**), in the cross section of the straight rectangular waveguide. In addition, we can find the thickness of the dielectric layer that is recommended to obtain the desired behavior of the output fields.

Several examples will demonstrate in the next section in order to understand the influence of the hollow rectangular waveguide with dielectric material in the cross section (**Figure 1**) on the output field. All the graphical results will be demonstrated as a response to a half-sine (TE_{10}) input-wave profile and the hollow rectangular waveguide with dielectric material in the cross section of the straight rectangular waveguide.

4. The derivation for circular straight waveguide

The wave Eqs. (1) and (2) are given in the case of the circular straight waveguide, where

$$\varepsilon(r) = \varepsilon_0[1 + \chi_0 g(r)] \text{ and } g_r(r) = [1/\varepsilon(r)][\partial \varepsilon(r)/\partial r].$$

The proposed technique to calculate the refractive index for discontinuous problems (**Figure 1(f)** and **(g)**) is given in this section for the one dielectric coating (**Figure 1(f)**) and for three dielectric coatings (**Figure 1(g)**).

4.1 The refractive index for the circular hollow waveguide with one dielectric coating in the cross section

The cross section of the hollow waveguide (**Figure 1(f)**) is made of a tube of various types of one dielectric layer and a metallic layer. The refractive indices of

the air, dielectric, and metallic layers are $n_{(0)} = 1$, $n_{(AgI)} = 2$, and $n_{(Ag)} = 10 - j60$, respectively. The value of the refractive index of the material at a wavelength of $\lambda = 10.6 \mu\text{m}$ is taken from the table performed by Miyagi et al. [19]. The refractive indices of the air, dielectric layer (AgI), and metallic layer (Ag) are shown in **Figure 1(f)**.

The refractive index ($n(r)$) is dependent on the transition's regions in the cross section between the two different materials (air-AgI, AgI-Ag).

The refractive index is calculated as follows:

$$n(r) = \begin{cases} n_0 & 0 \leq r < b - \varepsilon_1/2 \\ n_0 + (n_d - n_0) \exp \left[1 - \frac{\varepsilon_1^2}{\varepsilon_1^2 - [r - (b + \varepsilon_1/2)]^2} \right] & b - \varepsilon_1/2 \leq r < b + \varepsilon_1/2 \\ n_d & b + \varepsilon_1/2 \leq r < a - \varepsilon_2/2, \\ n_d + (n_m - n_d) \exp \left[1 - \frac{\varepsilon_2^2}{\varepsilon_2^2 - [r - (a + \varepsilon_2/2)]^2} \right] & a - \varepsilon_2/2 \leq r < a + \varepsilon_2/2 \\ n_m & \text{else} \end{cases}$$

where the internal and external diameters are denoted as $2b$, $2a$, and $2(a + \delta_m)$, respectively, where δ_m is the metallic layer. The thickness of the dielectric coating (d) is defined as $[a - b]$, and the thickness of the metallic layer (δ_m) is defined as $[(a + \delta_m) - a]$. The parameter ε is very small [$\varepsilon = [a - b]/50$]. The refractive indices of the air, dielectric, and metallic layers are denoted as n_0 , n_d , and n_m , respectively.

4.2 The refractive index for the circular hollow waveguide with three dielectric coatings in the cross section

The cross section of the hollow waveguide (**Figure 1(g)**) is made of a tube of various types of three dielectric layers and a metallic layer. The internal and external diameters are denoted as $2b$, $2b_1$, $2b_2$, $2a$, and $2(a + \delta_m)$, respectively, where δ_m is the thickness of the metallic layer. In addition, we denote the thickness of the dielectric layers as d_1 , d_2 , and d_3 , respectively, where $d_1 = b_1 - b$, $d_2 = b_2 - b_1$, and $d_3 = a - b_2$. The refractive index in the particular case with the three dielectric layers and the metallic layer in the cross section of the straight hollow waveguide (**Figure 1(g)**) is calculated as follows:

$$n(r) = \begin{cases} n_0 & 0 \leq r < b - \varepsilon/2 \\ n_0 + (n_1 - n_0) \exp \left[1 - \frac{\varepsilon^2}{\varepsilon^2 - [r - (b + \varepsilon/2)]^2} \right] & b - \varepsilon/2 \leq r < b + \varepsilon/2 \\ n_1 & b + \varepsilon/2 \leq r < b_1 - \varepsilon/2 \\ n_1 + (n_2 - n_1) \exp \left[1 - \frac{\varepsilon^2}{\varepsilon^2 - [r - (b_1 + \varepsilon/2)]^2} \right] & b_1 - \varepsilon/2 \leq r < b_1 + \varepsilon/2 \\ n_2 & b_1 + \varepsilon/2 \leq r < b_2 - \varepsilon/2, \\ n_2 + (n_3 - n_2) \exp \left[1 - \frac{\varepsilon^2}{\varepsilon^2 - [r - (b_2 + \varepsilon/2)]^2} \right] & b_2 - \varepsilon/2 \leq r < b_2 + \varepsilon/2 \\ n_3 & b_2 + \varepsilon/2 \leq r < a - \varepsilon/2 \\ n_3 + (n_m - n_3) \exp \left[1 - \frac{\varepsilon^2}{\varepsilon^2 - [r - (a + \varepsilon/2)]^2} \right] & a - \varepsilon/2 \leq r < a + \varepsilon/2 \\ n_m & \text{else} \end{cases}$$

where the parameter ε is very small [$\varepsilon = [a - b]/50$]. The refractive indices of the air, dielectric, and metallic layers are denoted as n_0 , n_1 , n_2 , n_3 , and n_m , respectively. In this study we suppose that $n_3 > n_2 > n_1$.

The proposed technique to calculate the refractive indices of the dielectric profile of one dielectric coating (**Figure 1(f)**) or three dielectric coatings (**Figure 1(g)**), and the metallic layer in the cross section relate to the method that is based on Maxwell's equations, the Fourier-Bessel series, Laplace transform, and the inverse Laplace transform by the residue method [17]. This method becomes an improved method by using the proposed technique also in the cases of discontinuous problems of the hollow circular waveguide with one dielectric coating (**Figure 1(f)**), three dielectric coatings (**Figure 1(g)**), or more dielectric coatings.

5. Numerical results

Several examples for the rectangular and circular waveguides with the discontinuous dielectric profile in the cross section of the straight waveguide are demonstrated in this section according to **Figure 1(a)–(g)**.

Figure 4(a)–(c) demonstrates the output field as a response to a half-sine (TE_{10}) input-wave profile in the case of the slab profile (**Figure 1(a)**), where $a = b = 20$ mm, $c = 20$ mm, and $d = 2$ mm, for $\varepsilon_r = 3$, 4, and 5, respectively. **Figure 4(c)** shows the output field for $\varepsilon_r = 3$, 4, and 5, respectively, where $y = b/2 = 10$ mm.

By increasing only the value of the dielectric profile from $\varepsilon_r = 3$ to $\varepsilon_r = 5$, the width of the output field decreased, and also the output amplitude decreased.

Figure 5(a)–(e) demonstrates the output field as a response to a half-sine (TE_{10}) input-wave profile in the case of the rectangular dielectric profile in the rectangular waveguide (**Figure 1(b)**), where $a = b = 20$ mm and $c = d = 2$ mm, for $\varepsilon_r = 3$, 5, 7, and 10, respectively. **Figure 5(e)** shows the output field for $\varepsilon_r = 3$, 5, 7, and 10, respectively, where $y = b/2 = 10$ mm.

By increasing only the dielectric profile from $\varepsilon_r = 3$ to $\varepsilon_r = 5$, the width of the output field increased, and also the output amplitude increased.

The output fields are strongly affected by the input-wave profile (TE_{10} mode), the location, and the dielectric profile, as shown in **Figure 4(a)–(c)** and **Figure 5(a)–(e)**.

Figure 6(a)–(e) shows the output field as a response to a half-sine (TE_{10}) input-wave profile in the case of the circular dielectric profile (**Figure 1(c)**), for $\varepsilon_r = 3$, 5, 7 and 10, respectively, where $a = b = 20$ mm, and the radius of the circular dielectric profile is equal to 1 mm. **Figure 6(e)** shows the output field for $\varepsilon_r = 3$, 5, 7, and 10, respectively, where $y = b/2 = 10$ mm. The other parameters are $z = 0.15$ m, $k_0 = 167$ 1/m, $\lambda = 3.75$ cm, and $\beta = 58$ 1/m.

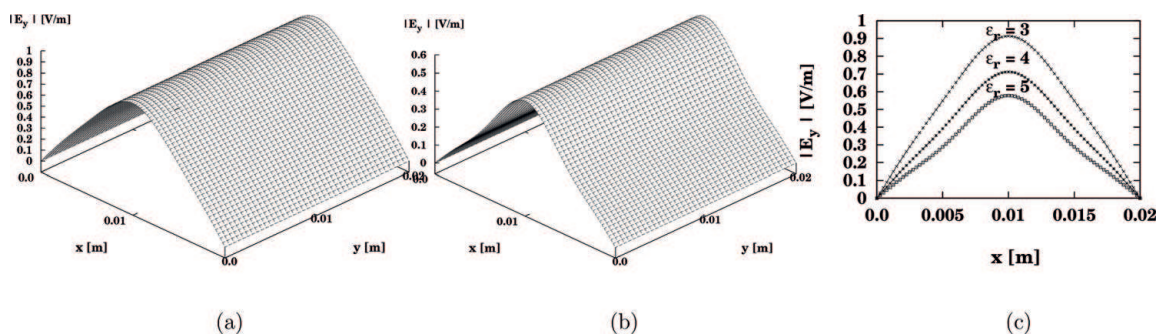


Figure 4.

The output field as a response to a half-sine (TE_{10}) input-wave profile in the case of the slab dielectric profile (**Figure 1(a)**), where $a = b = 20$ mm, $c = 20$ mm, and $d = 2$ mm where (a) $\varepsilon_r = 3$ and (b) $\varepsilon_r = 5$. (c). The output field for $\varepsilon_r = 3$, 4, and 5, respectively, where $y = b/2 = 10$ mm.

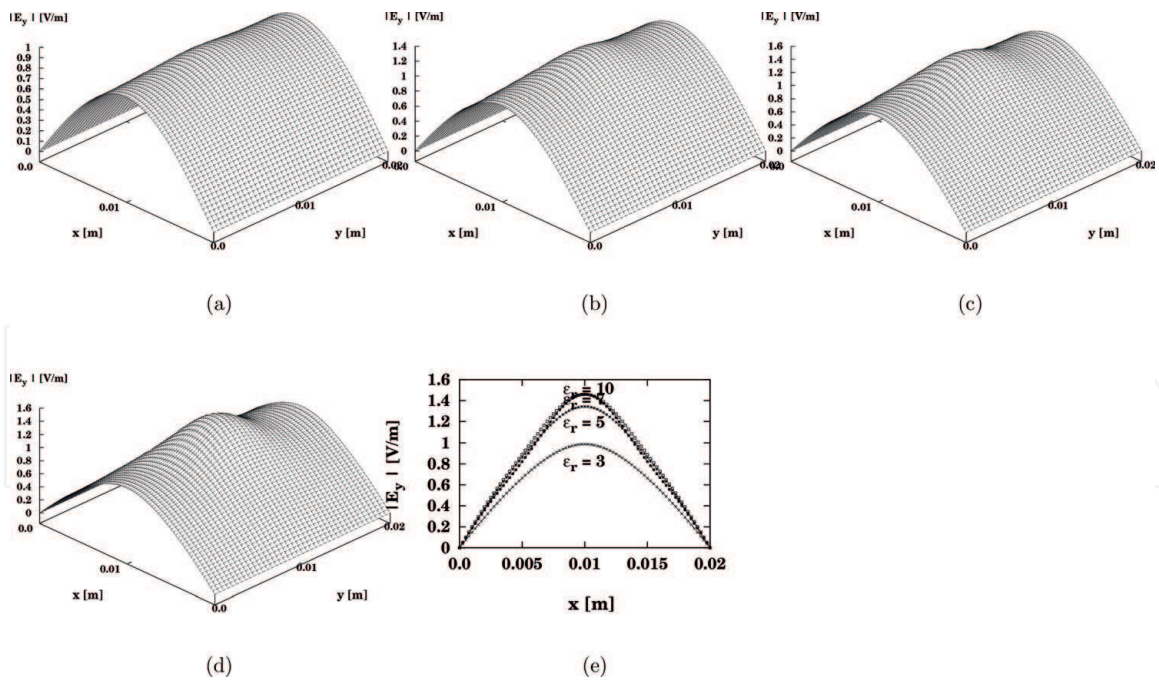


Figure 5. The output field as a response to a half-sine (TE_{10}) input-wave profile in the case of the rectangular dielectric material (**Figure 1(b)**), where $a = b = 20$ mm and $c = d = 2$ mm: (a) $\epsilon_r = 3$, (b) $\epsilon_r = 5$, (c) $\epsilon_r = 7$, and (d) $\epsilon_r = 10$. The other parameters are $a = b = 20$ mm, $z = 0.15$ m, $k_0 = 167$ 1/m, $\lambda = 3.75$ cm, and $\beta = 58$ 1/m. (e) The output field for $\epsilon_r = 3, 5, 7$, and 10 , respectively, where $y = b/2 = 10$ mm.

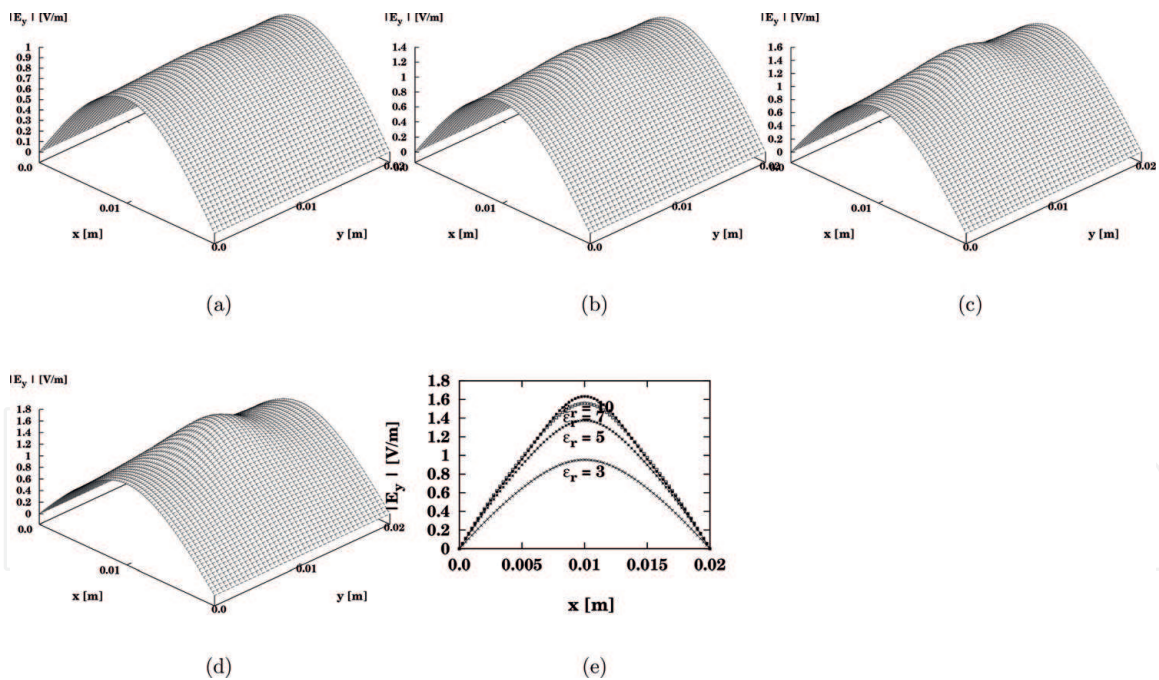


Figure 6. The output field as a response to a half-sine (TE_{10}) input-wave profile in the case of the circular dielectric profile (**Figure 1(c)**), where $a = b = 20$ mm, and the radius of the circular dielectric profile is equal to 1 mm: (a) $\epsilon_r = 3$, (b) $\epsilon_r = 5$, (c) $\epsilon_r = 7$, and (d) $\epsilon_r = 10$. The other parameters are $z = 0.15$ m, $k_0 = 167$ 1/m, $\lambda = 3.75$ cm, and $\beta = 58$ 1/m. (e) The output field for $\epsilon_r = 3, 5, 7$, and 10 , respectively, where $y = b/2 = 10$ mm.

The proposed technique in Section 3.3 is also effective to solve discontinuous problems of periodic circular profiles in the cross section of the straight rectangular waveguides, and some examples were demonstrated in Ref. [20].

The behavior of the output fields (**Figures 5(a)–(e)** and **6(a)–(e)**) is similar when the dimensions of the rectangular dielectric profile (**Figure 1(b)**) and the circular profile (**Figure 1(c)**) are very close. The output field (**Figure 5(a)–(e)**) is

shown for $c = d = 2$ mm as regards to the dimensions $a = b = 20$ mm. The output field (**Figure 6(a)–(e)**) is shown where the radius of circular profile is equal to 1 mm (viz., the diameter 2 mm), as regards to the dimensions $a = b = 20$ mm.

Figure 7(a)–(e) shows the output field as a response to a half-sine (TE_{10}) input-wave profile in the case of the circular dielectric profile (**Figure 1(c)**), where $a = b = 20$ mm, and the radius of the circular dielectric profile is equal to 2 mm for $\epsilon_r = 3, 5, 7$, and 10, respectively. The other parameters are $z = 0.15$ m, $k_0 = 167$ 1/m, $\lambda = 3.75$ cm, and $\beta = 58$ 1/m. **Figure 7(e)** shows the output field for $\epsilon_r = 3, 5, 7$, and 10, respectively, where $y = b/2 = 10$ mm.

By changing only the value of the radius of the circular dielectric profile (**Figure 1(c)**) from 1 mm to 2 mm, as regards to the dimensions of the cross section of the waveguide ($a = b = 20$ mm), the output field of the Gaussian shape increased, and the half-sine (TE_{10}) input-wave profile decreased.

The dielectric profile of the hollow rectangular waveguide with the dielectric material between the hollow rectangle and the metal (**Figure 1(e)**) is calculated by subtracting the dielectric profile of the waveguide with the dielectric material in the core (**Figure 1(b)**) from the dielectric profile according to the waveguide entirely with the dielectric profile (**Figure 1(d)**).

Figure 8(a)–(c) shows the output field as a response to a half-sine (TE_{10}) input-wave profile in the case of the hollow rectangular waveguide with one dielectric material between the hollow rectangle and the metal (**Figure 1(e)**), where $a = b = 20$ mm, $c = d = 14$ mm, and $d = 14$ mm, namely, $e = 3$ mm and $f = 3$ mm. **Figure 8(a)–(b)** shows the output field for $\epsilon_r = 2.5$ and $\epsilon_r = 4$, respectively. **Figure 8(c)** shows the output field for $\epsilon_r = 2.5, 3, 3.5$, and 4, respectively, where $y = b/2 = 10$ mm. The other parameters are $z = 0.15$ m, $k_0 = 167$ 1/m, $\lambda = 3.75$ cm, and $\beta = 58$ 1/m.

Figure 9(a)–(c) shows the output power density in the case of the hollow circular waveguide with one dielectric coating (**Figure 1(f)**), where $a = 0.5$ mm. **Figure 9(a)–(b)** shows the output power density for $w_0 = 0.15$ mm and $w_0 = 0.25$ mm, respectively. The output power density of the central peak is shown

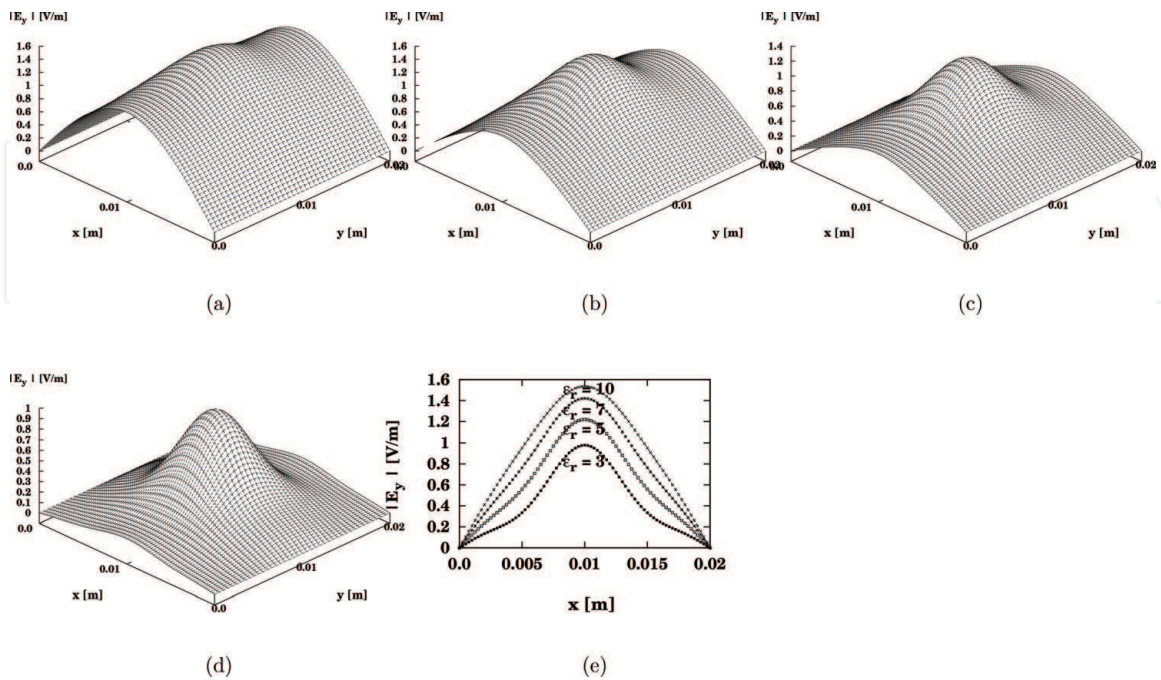


Figure 7.

The output field as a response to a half-sine (TE_{10}) input-wave profile in the case of the circular dielectric profile (**Figure 1(c)**), where $a = b = 20$ mm, and the radius of the circular dielectric profile is equal to 2 mm: (a) $\epsilon_r = 3$, (b) $\epsilon_r = 5$, (c) $\epsilon_r = 7$, and (d) $\epsilon_r = 10$. The other parameters are $z = 0.15$ m, $k_0 = 167$ 1/m, $\lambda = 3.75$ cm, and $\beta = 58$ 1/m. (e) The output field for $\epsilon_r = 3, 5, 7$, and 10, respectively, where $y = b/2 = 10$ mm.

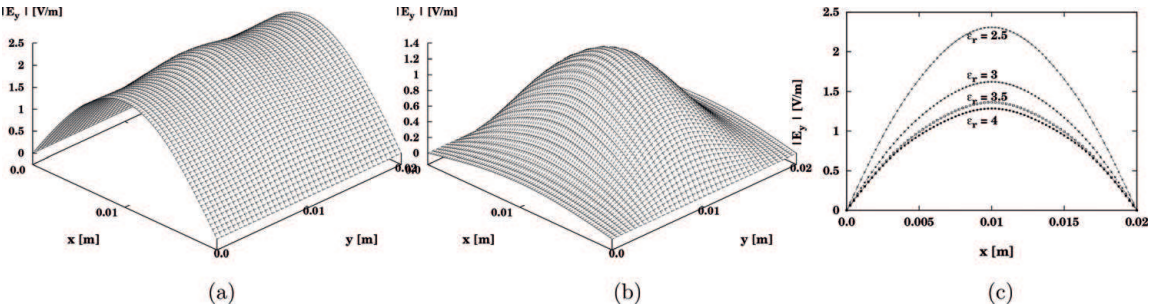


Figure 8.
 The output field as a response to a half-sine (TE_{10}) input-wave profile in the case of the hollow rectangular waveguide with one dielectric material between the hollow rectangle and the metal (**Figure 1(e)**), where $a = b = 20\text{ mm}$, $c = 14\text{ mm}$, and $d = 14\text{ mm}$, namely, $e = 3\text{ mm}$ and $f = 3\text{ mm}$: (a) $\epsilon_r = 2.5$, and (b) $\epsilon_r = 4$. (c). The output field for $\epsilon_r = 2.5, 3, 3.5$, and 4 , respectively, where $y = b/2 = 10\text{ mm}$. The other parameters are $z = 0.15\text{ m}$, $k_0 = 167\text{ 1/m}$, $\lambda = 3.75\text{ cm}$, and $\beta = 58\text{ 1/m}$.

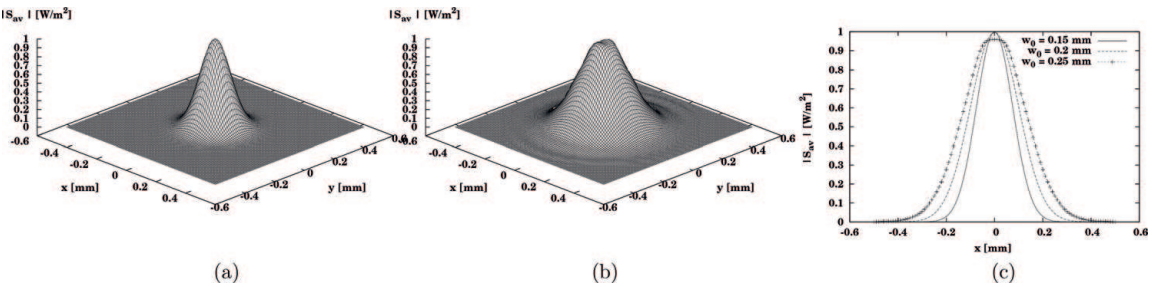


Figure 9.
 The output power density in the case of the hollow circular waveguide with one dielectric coating (**Figure 1(e)**), where $a = 0.5\text{ mm}$: (a) $w_0 = 0.15\text{ mm}$, and (b) $w_0 = 0.25\text{ mm}$. (c). The output power density of the central peak for $w_0 = 0.15\text{ mm}$, $w_0 = 0.2\text{ mm}$, and $w_0 = 0.25\text{ mm}$, respectively, where $y = b/2$. The other parameters are $z = 1\text{ m}$, $n_d = 2.2$, and $n_{(Ag)} = 13.5 - j\,75.3$.

for $w_0 = 0.15\text{ mm}$, $w_0 = 0.2\text{ mm}$, and $w_0 = 0.25\text{ mm}$, respectively, where $y = b/2$. The other parameters are $z = 1\text{ m}$, $n_d = 2.2$, and $n_{(Ag)} = 13.5 - j\,75.3$.

Figure 1(f) and **(g)** shows two examples of discontinuous problems for circular waveguides. The practical results are demonstrated for **Figure 1(f)**.

Figure 10(a)–(c) shows also the output power density in the case of the hollow circular waveguide with one dielectric coating (**Figure 1(f)**), where $a = 0.5\text{ mm}$, but for other values of the spot size. **Figure 10(a)–(b)** shows the output power density for $w_0 = 0.26\text{ mm}$ and $w_0 = 0.3\text{ mm}$, respectively. The output power density of the central peak is shown for $w_0 = 0.26\text{ mm}$, $w_0 = 0.28\text{ mm}$, and $w_0 = 0.3\text{ mm}$, respectively, where $y = b/2$. The other parameters are $z = 1\text{ m}$, $n_d = 2.2$, and $n_{(Ag)} = 13.5 - j\,75.3$.

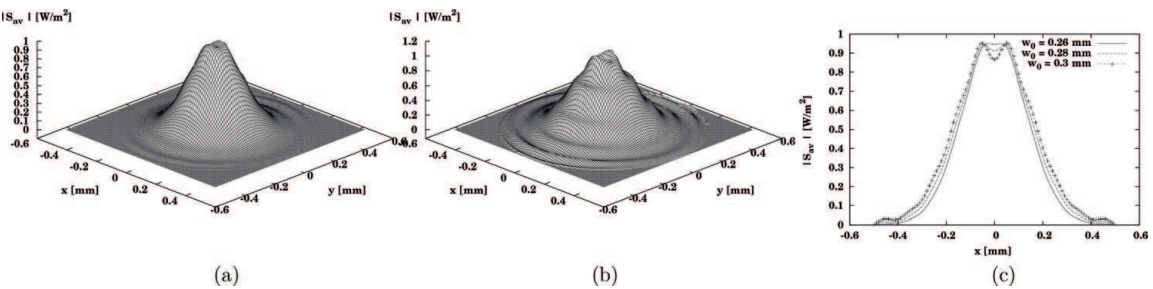


Figure 10.
 The output power density in the case of the hollow circular waveguide with one dielectric coating (**Figure 1(e)**), where $a = 0.5\text{ mm}$: (a) $w_0 = 0.26\text{ mm}$, and (b) $w_0 = 0.3\text{ mm}$. (c). The output power density of the central peak for $w_0 = 0.26\text{ mm}$, $w_0 = 0.28\text{ mm}$, and $w_0 = 0.3\text{ mm}$, respectively, where $y = b/2$. The other parameters are $z = 1\text{ m}$, $n_d = 2.2$, and $n_{(Ag)} = 13.5 - j\,75.3$.

By changing only the values of the spot size from $w_0 = 0.15$ mm, $w_0 = 0.2$ mm, and $w_0 = 0.25$ mm to $w_0 = 0.26$ mm, $w_0 = 0.28$ mm, and $w_0 = 0.3$ mm, respectively, the results of the output power density for $a = 0.5$ mm are changed as shown in **Figure 10(a)–10(c)**.

The output modal profile is greatly affected by the parameters of the spot size and the dimensions of the cross section of the waveguide. **Figure 10(a)–(c)** demonstrates that in addition to the main propagation mode, several other secondary modes and symmetric output shape appear in the results of the output power density for the values of $w_0 = 0.26$ mm, $w_0 = 0.28$ mm, and $w_0 = 0.3$ mm, respectively.

The proposed technique in Section 4.2 is also effective to solve discontinuous problems of the straight hollow circular waveguide with three dielectric layers (**Figure 1(g)**), and some examples were demonstrated in Ref. [21].

6. Conclusions

Several examples for the rectangular and circular waveguides with the discontinuous dielectric profile in the cross section of the straight waveguide were demonstrated in this research, according to **Figure 1(a)–(g)**.

Figure 4(a)–(c) demonstrates the output field as a response to a half-sine (TE_{10}) input-wave profile in the case of the slab profile (**Figure 1(a)**), where $a = b = 20$ mm, $c = 20$ mm, and $d = 2$ mm for $\epsilon_r = 3$ and 5, respectively. By increasing only the value of the dielectric profile from $\epsilon_r = 3$ to $\epsilon_r = 5$, the width of the output field decreased, and also the output amplitude decreased.

Figure 5(a)–(e) demonstrates the output field as a response to a half-sine (TE_{10}) input-wave profile in the case of the rectangular dielectric profile in the rectangular waveguide (**Figure 1(b)**), where $a = b = 20$ mm and $c = d = 2$ mm, for $\epsilon_r = 3, 5, 7$, and 10, respectively. By increasing only the dielectric profile from $\epsilon_r = 3$ to $\epsilon_r = 5$, the width of the output field increased, and also the output amplitude increased. The output fields are strongly affected by the input-wave profile (TE_{10} mode), the location, and the dielectric profile, as shown in **Figure 4(a)–(c)** and **Figure 5(a)–(e)**.

The behavior of the output fields (**Figures 5(a)–(e)** and **6(a)–(e)**) is similar when the dimensions of the rectangular dielectric profile (**Figure 1(b)**) and the circular profile (**Figure 1(c)**) are very close. The output field (**Figure 5(a)–(e)**) is shown for $c = d = 2$ mm as regards to the dimensions $a = b = 20$ mm. The output field (**Figure 6(a)–(e)**) is shown where the radius of circular profile is equal to 1 mm (viz., the diameter 2 mm), as regards to the dimensions $a = b = 20$ mm.

Figures 6(a)–(e) and **7(a)–(e)** show the output field as a response to a half-sine (TE_{10}) input-wave profile in the case of the circular dielectric profile (**Figure 1(c)**), for $\epsilon_r = 3, 5, 7$, and 10, respectively, where $a = b = 20$ mm, and the radius of the circular dielectric profile is equal to 1 mm. By changing only the value of the radius of the circular dielectric profile (**Figure 1(c)**) from 1 mm to 2 mm, as regards to the dimensions of the cross section of the waveguide ($a = b = 20$ mm), the output field of the Gaussian shape increased, and the half-sine (TE_{10}) input-wave profile decreased.

Figure 8(a)–(c) shows the output field as a response to a half-sine (TE_{10}) input-wave profile in the case of the hollow rectangular waveguide with one dielectric material between the hollow rectangle and the metal (**Figure 1(e)**), where $a = b = 20$ mm, $c = d = 14$ mm, and $d = 14$ mm, namely, $e = 3$ mm and $f = 3$ mm.

Figures 9(a)–(c) and **10(a)–(c)** show the output power density in the case of the hollow circular waveguide with one dielectric coating (**Figure 1(f)**), where $a = 0.5$ mm. By changing only the values of the spot size from $w_0 = 0.15$ mm, $w_0 = 0.2$ mm, and $w_0 = 0.25$ to $w_0 = 0.26$ mm, $w_0 = 0.28$ mm, and $w_0 = 0.3$ mm,

respectively, the results of the output power density for $a = 0.5$ mm are changed as shown in **Figure 10(a)–(c)**.

The output modal profile is greatly affected by the parameters of the spot size and the dimensions of the cross section of the waveguide. **Figure 10(a)–(c)** demonstrates that in addition to the main propagation mode, several other secondary modes and symmetric output shape appear in the results of the output power density for the values of $w_0 = 0.26$ mm, $w_0 = 0.28$ mm, and $w_0 = 0.3$ mm, respectively.


The two important parameters that we studied were the spot size and the dimensions of the cross section of the straight hollow waveguide. The output results are affected by the parameters of the spot size and the dimensions of the cross section of the waveguide.

Author details

Zion Menachem
Department of Electrical Engineering, Sami Shamoon College of Engineering,
Beer Sheva, Israel

*Address all correspondence to: zionm@post.tau.ac.il

IntechOpen

© 2018 The Author(s). Licensee IntechOpen. This chapter is distributed under the terms of the Creative Commons Attribution License (<http://creativecommons.org/licenses/by/3.0>), which permits unrestricted use, distribution, and reproduction in any medium, provided the original work is properly cited. 

References

- [1] Chiang KS. Review of numerical and approximate methods for the modal analysis of general optical dielectric waveguides. *Optical and Quantum Electronics*. 1993;**26**: S113-S134
- [2] Mineo M, Carlo AD, Paoloni C. Analytical design method for corrugated rectangular waveguide SWS THZ vacuum tubes. *Journal of Electromagnetic Waves and Applications*. 2010;**24**:2479-2494
- [3] Yeap KH, Tham CY, Yassin G, Yeong KC. Attenuation in rectangular waveguides with finite conductivity walls. *Radioengineering*. 2011;**20**: 472-478
- [4] Liu S, Li LW, Leong MS, Yeo T Sr. Rectangular conducting waveguide filled with uniaxial anisotropic media: A modal analysis and dyadic Green's function. *Progress in Electromagnetics Research*. 2000;**25**:111-129
- [5] Lu W, Lu YY. Waveguide mode solver based on Neumann-to-Dirichlet operators and boundary integral equations. *Journal of Computational Physics*. 2012;**231**:1360-1371
- [6] Chen TT. Wave propagation in an inhomogeneous transversely magnetized rectangular waveguide. *Applied Scientific Research*. 1960;**8**: 141-148
- [7] Vaish A, Parthasarathy H. Analysis of a rectangular waveguide using finite element method. *Progress in Electromagnetics Research C*. 2008;**2**: 117-125
- [8] Khalaj-Amirhosseini M. Microwave filters using waveguides filled by multi-layer dielectric. *Progress in Electromagnetics Research, PIER*. 2006; **66**:105-110
- [9] Khalaj-Amirhosseini M. Analysis of longitudinally inhomogeneous waveguides using the method of moments. *Progress in Electromagnetics Research, PIER*. 2007;**74**:57-67
- [10] Khalaj-Amirhosseini M. Analysis of longitudinally inhomogeneous waveguides using Taylor's series expansion. *Journal of Electromagnetic Waves and Applications*. 2006;**16**: 1093-1100
- [11] Khalaj-Amirhosseini M. Analysis of longitudinally inhomogeneous waveguides using the Fourier series expansion. *Journal of Electromagnetic Waves and Applications*. 2006;**20**: 1299-1310
- [12] Harrington JA, Matsuura Y. Review of hollow waveguide technology. *SPIE*. 1995;**2396**:4-14
- [13] Harrington JA, Harris DM, Katzir A, editors. *Biomedical Optoelectronic Instrumentation*, 4-14; 1995
- [14] Harrington JA. A review of IR transmitting, hollow waveguides. *Fiber and Integrated Optics*. 2000;**19**:211-228
- [15] Marhic ME. Mode-coupling analysis of bending losses in IR metallic waveguides. *Applied Optics*. 1981;**20**: 3436-3441
- [16] Menachem Z, Jerby E. Transfer matrix function (TMF) for propagation in dielectric waveguides with arbitrary transverse profiles. *IEEE Transactions on Microwave Theory and Techniques*. 1998;**46**:975-982
- [17] Menachem Z, Tapuchi S. Influence of the spot-size and cross-section on the output fields and power density along the straight hollow waveguide. *Progress in Electromagnetics Research*. 2013;**48**: 151-173

[18] Vladimirov V. Equations of Mathematical Physics. New York: Marcel Dekker, Inc; 1971

[19] Miyagi M, Harada K, Kawakami S. Wave propagation and attenuation in the general class of circular hollow waveguides with uniform curvature. IEEE Transactions on Microwave Theory and Techniques. 1984;**MTT-32**: 513-521

[20] Menachem Z, Tapuchi S. Circular and periodic circular profiles in a rectangular cross section along the straight waveguide. Applied Physics Research. 2015;**7**:121-136

[21] Menachem Z, Tapuchi S. Straight hollow waveguide with three dielectric layers in the cross section. Journal of Electromagnetic Waves and Applications. 2016;**30**:2125-2137